Pergamon

Int. J. Heat Mass Transfer. Vol. 37, No. 9, pp. 1411–1420, 1994

0017-9310/94 $7.00+0.00

0017-9310(93)E0087-W

Wall heating effect on local heat transfer in a rotating two-pass square channel with 90° rib turbulators

JAMES A. PARSONS, JE-CHIN HAN and YUMING ZHANG

Turbine Heat Transfer Laboratory, Department of Mechanical Engineering, Texas A&M University, College Station, TX 77843-3123, U.S.A.

(*Received* 5 *February* 1993 *and in final form* 9 *November* 1993)

Abstract—The influence of wall heating condition on the local heat transfer coefficient in a rotating, two-pass, square channel with 90° transverse ribs on the leading and trailing walls was investigated for Reynolds numbers from 2500 to 25000 and rotation numbers from 0 to 0.352. Three thermal boundary condition cases were studied: (A) all four walls at the same temperature, (B) all four walls at the same heat flux, and (C) trailing wall hotter than leading with side walls unheated and insulated. The results for case A show that the ribbed wall heat transfer coefficients with rotation increase by a factor of two to three over the smooth wall data with rotation. As rotation number (or buoyancy parameter) increases, the heat transfer coefficients on the first pass (outflow) trailing wall increase and on the first pass leading wall decrease. The reverse is true for the second pass (inflow). The heat transfer coefficients on the first pass leading and second pass trailing walls for cases B and C are 50% higher than those for case A.

INTRODUCTION

THE HEAT load of the rotating turbine blades in a gas turbine engine poses a challenging problem in designing for blade life and performance. Several methods such as film cooling and augmented convective cooling in internal serpentine channels (shown in Fig. 1(a)) remove heat from the blades. This paper focuses on the influence of wall heating (thermal boundary) condition on local surface heat transfer coefficients in a rotating, two-pass, square channel with 90° transverse, rib-turbulated walls. Comparisons with other ribbed results are also discussed.

Previous investigations of turbine blade internal coolant passage heat transfer have concentrated on non-rotating models that do not account for the Coriolis force and the centrifugal buoyancy force effects on coolant motion and heat transfer [1, 2]. However, some researchers reported the effect of rotation on the heat transfer characteristics in a straight channel with smooth walls and radial outward flow [3–7]. References [8, 9] studied the effect of rotation on the heat transfer coefficients in a rectangular channel with ribbed walls and radial outward flow. References [10–13] systematically investigated the effect of rotation on the local heat transfer coefficient in a serpentine square coolant channel (three-pass) with smooth and ribbed walls, respectively, for parameters similar to typical engine conditions. Reference [14] also showed results for rotation effects on local heat transfer coefficient in a four-pass smooth square channel. Reference [15] predicted the channel fluid velocities and heat transfer coefficients in a rotating smooth channel with radial outward flow and agreed within 10–30% with data shown in ref. [10].

In summary, for the case of a multi-pass smooth wall channel, refs. [10, 11] reported that the rotating trailing surface heat transfer coefficient of the first coolant pass (radial outward flow) increased up to 3.5 times the stationary fully developed circular tube values, but the leading surface heat transfer coefficient decreased to 40% of the stationary tube values. However, the rotating trailing surface heat transfer coefficient of the second coolant pass (radial inward flow) decreased by 30% compared to the stationary tube values, while the leading surface heat transfer coefficient increased by 100%, compared to the stationary tube results. For the case of a multi-pass, square channel with trips normal to the flow (90° transverse ribs), ref. [12] showed that the maximum rotating heat transfer coefficient increased up to 4.5 times from the stationary fully developed circular tube values, above the highest levels for the rotating smooth wall (~3.5 times). However, the minimum rotating heat transfer coefficients decreased to 80% of the non-rotating 90° ribbed wall results. For the case of a multi-pass square channel with trips skewed to the flow (45° ribs), ref. [13] concluded that the maximum rotating heat transfer coefficient increased up to 5.0 times of the stationary tube values, while the minimum rotating heat transfer coefficient decreased to 40% of the non-rotating 45° ribbed wall values.

References [16, 17] reported the effect of wall heating condition on local heat transfer coefficients in a one-pass and two-pass square channel with smooth

NOMENCLATURE

A	projected heat transfer surface area
D	hydraulic diameter; square channel width or height
e	rib height
h	heat transfer coefficient
k	thermal conductivity of coolant (air)
L	heated channel length (each pass)
Nu	local Nusselt number, hD/k
$\bar{Nu}$	pass averaged Nusselt number
Nu_0	Nusselt number in fully developed turbulent tube flow
P	rib pitch or streamwise spacing
Pr	Prandtl number
q_{net}	net heat transfer rate
q''	net heat transfer flux
R	local rotating radius
$\bar{R}$	mean rotating radius
Re	Reynolds number, $\rho DV/\mu$
Ro	rotation number, $\Omega D/V$
T_b	local bulk mean coolant temperature
T_{bi}	inlet bulk mean coolant temperature
T_w	local wall temperature
T_{wA}	local wall temperature of sidewall A
T_{wB}	local wall temperature of sidewall B
T_{wL}	local wall temperature of leading wall
T_{wT}	local wall temperature of trailing wall
V	mean coolant channel velocity
X	channel axial distance from heated channel inlet
X'	channel axial distance from second pass inlet.

Greek symbols

$\Delta\rho/\rho$	coolant-to-wall density ratio based on local bulk mean coolant temperature, $(\rho_b-\rho_w)/\rho_b = (T_w-T_b)/T_w$
$(\Delta\rho/\rho)_i$	coolant-to-wall density ratio based on inlet bulk mean coolant temperature, $(\rho_{bi}-\rho_w)/\rho_{bi} = (T_w-T_{bi})/T_w$
μ	coolant dynamic viscosity
ρ	coolant density
ρ_b	coolant density based on local bulk mean coolant temperature
ρ_{bi}	coolant density based on inlet bulk mean coolant temperature
ρ_w	coolant density based on local wall temperature
Ω	rotational speed, r.p.m.

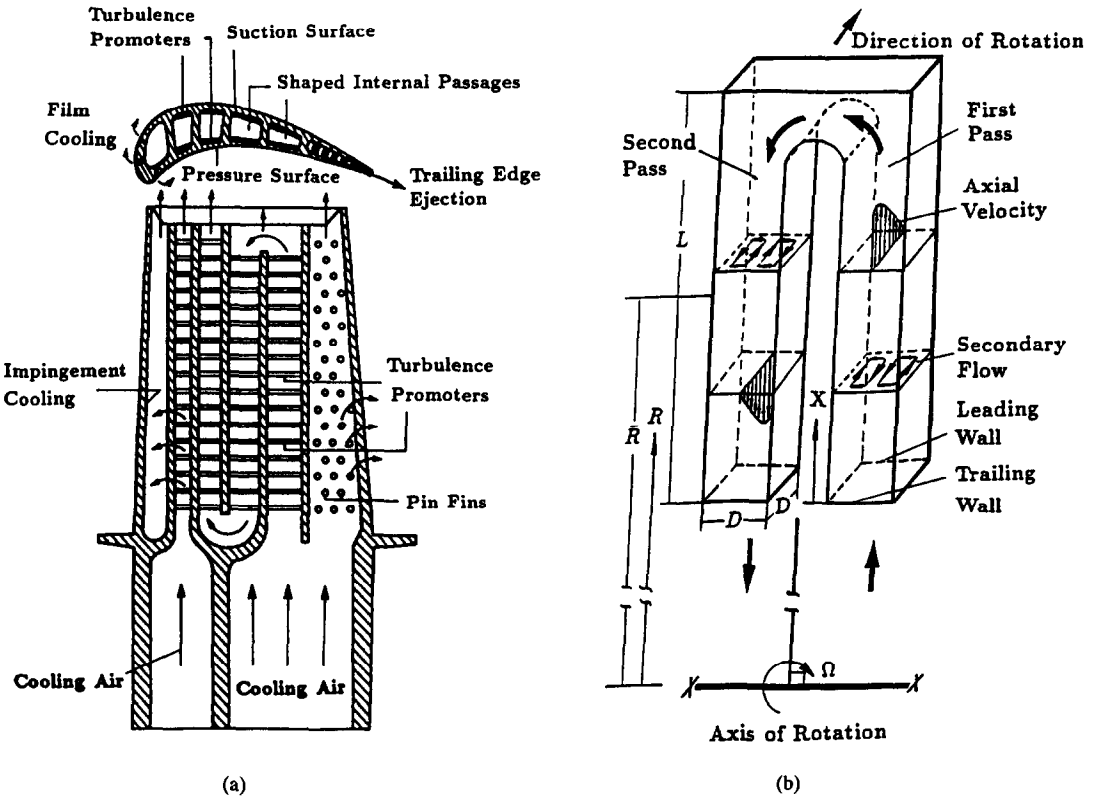

FIG. 1. (a) Cooling concepts of a modern multipass turbine blade. (b) Conceptual view of a two-pass rotating coolant velocity profile.

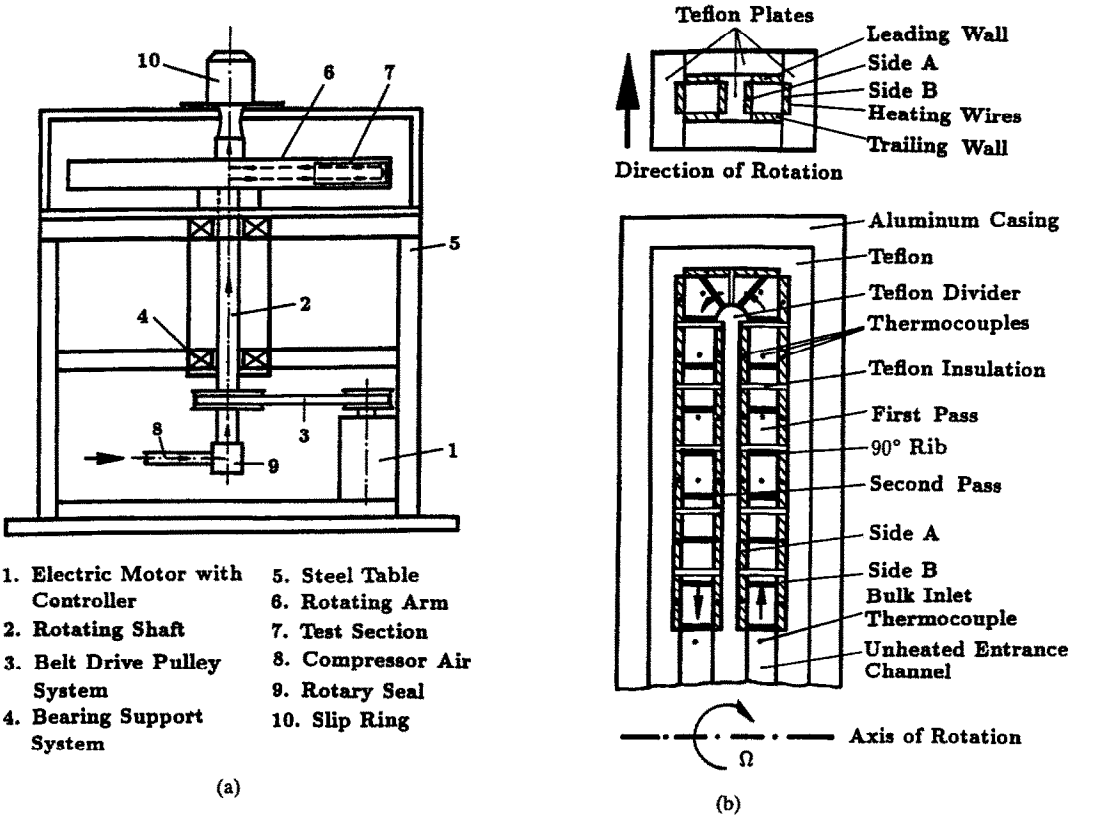

FIG. 2. (a) Schematic of the rotating rig. (b) Schematic of the two-pass heat transfer test model.

walls (shown in Fig. 1(b)). Their rotating smooth-wall heat transfer results agreed with refs. [10, 11] for the case of uniform wall temperature conditions, all walls at the same temperature. However, refs. [16, 17] found that for the uniform wall heat flux and simulated engine wall heating conditions, the rotating leading surface heat transfer coefficients of the first coolant pass (radial outward flow) and the rotating trailing surface heat transfer coefficients of the second coolant pass (radial inward flow) were up to 100% greater than those for the uniform wall temperature conditions. Since wall heating condition significantly affects rotating smooth wall channel heat transfer, it is unknown how effects due to wall heating condition change when ribs are installed to the channel walls. Therefore, the objective of this study is to investigate the effects of wall heating condition on local surface heat transfer coefficients in a rotating two-pass square channel with 90° transverse ribs on the leading and trailing walls. Three wall heating conditions were tested: Case (A) four walls at the same temperature, Case (B) four walls at the same heat flux, and Case (C) the trailing wall hotter than the leading wall but with two side walls unheated and insulated (to simulate turbine engine operating conditions).

EXPERIMENTAL FACILITY

The test stand (Fig. 2(a)) has been described and illustrated in refs. [16, 17]. A short description follows. Regulated compressor air flows from an orifice meter and passes through a hollow rotating shaft and a hollow rotating arm, which is mounted perpendicularly onto the shaft. The air then enters the test model (a ribbed, two-pass, square channel at the outer radius of the arm) and is exhausted into the atmosphere at the opposite end of the rotating shaft. Slip ring units transfer thermocouple outputs to a data logger interfaced to a personal computer, and transfer variac transformer outputs to wire resistance heaters uniformly cemented in grooves on the back of the test model's copper plates. An electric motor with an adjustable frequency controller turns the shaft, arm and test model via a toothed belt. The rotating shaft speed is measured by a digital photo tachometer.

To obtain regionally averaged heat transfer coefficients for turbine cooling design it is desirable to have a test model with regions isolated in the channel streamwise and circumferential directions. The two-pass square channel test model is divided into twelve short copper sections, six per pass (Fig. 2(b)). Each copper section is composed of four copper plates and has an inner cross section of 1.27 cm by 1.27 cm (1/2 in. by 1/2 in.). Thin Teflon strips are machined along the periphery contact surface between copper sections for insulation to significantly reduce heat conduction among copper plates. The square test channel's total length-to-hydraulic diameter ratio is 24, while each pass length-to-hydraulic diameter ratio (L/D) is 12. The ratio of the mean rotating arm radius to the

channel hydraulic diameter ($\bar{R}/D$) is 30. The ribbed trailing and leading surfaces are made by gluing brass ribs of square cross section to the copper plates. The thickness of the conductive glue is less than 0.01 cm and creates a negligible thermal insulation effect between the ribs and the copper plates. For this study, the rib height-to-hydraulic diameter ratio (e/D) is 0.125, the rib pitch-to-height ratio (P/e) is 10, and the ribs are transverse (the angle between the rib and coolant flow direction, pass axis, equals 90°). The ribs, only on the leading and trailing walls, are directly opposite (not staggered). The smooth side walls are isolated from the leading and trailing walls to eliminate heat conduction. Each wall has its own heater powered by a variac transformer for controllable heat flux and thus temperature. The entire heated test channel is insulated by Teflon material and fits in the hollow cylindrical arm for structural integrity. The local wall temperature of the test model is measured by 48 copper–constantan thermocouples distributed along the length and around the perimeter of the copper channel. They lie just below the channel surface and are glued in blind holes on the back side of each copper plate. Two more thermocouples measure the inlet and outlet bulk air temperature. The model has an unheated Teflon entrance channel (partially shown in Fig. 2(b)) that has the same cross section and length as one pass of the channel. This serves to establish hydrodynamically fully developed flow at the entrance to the heated channel.

DATA REDUCTION

The local heat transfer coefficient is calculated from the local net heat transfer rate per unit projected surface area to the cooling air, the local wall temperature on each copper plate, and the local bulk mean air temperature as:

$$h = q_{net}/[A/(T_w - T_b)]. \quad (1)$$

Local net heat transfer rate (q_{net}) is the electrical power generated by the heaters, calculated from heater voltage and current measurements, minus the power loss by conduction through the Teflon and away from the channel. Tests to find this loss are conducted without air flow for non-rotating and rotating conditions and for each wall heating condition (Cases A, B, and C), by taking simultaneous measurements for each test model wall. Several different power input levels are used to obtain the power loss relationships for each wall as a function of its temperature at steady state. To place the results on a common basis, the heat transfer area used in equation (1) is always that of a smooth wall, i.e. the wetted area increase due to the ribs is not included.

The local wall temperatures in equation (1) are from the thermocouples in each copper plate. The local bulk mean air temperature uses the corresponding X/L (or X'/L) for each thermocouple location in interpolating between the measured inlet (about 30°C) and exit bulk temperatures. The total net heat transfer rate from the test channel to the cooling air agreed with the bulk mean air temperature rise along the test channel for Reynolds numbers larger than 5000 (i.e. an energy balance was achieved). Figure 3 shows typical variations of local wall-to-bulk mean air temperature along the two-pass test channel for two different wall heating conditions (Cases A and B) at rotation numbers of 0.0 and 0.088 (0 and 800 r.p.m. at $Re = 10\,000$).

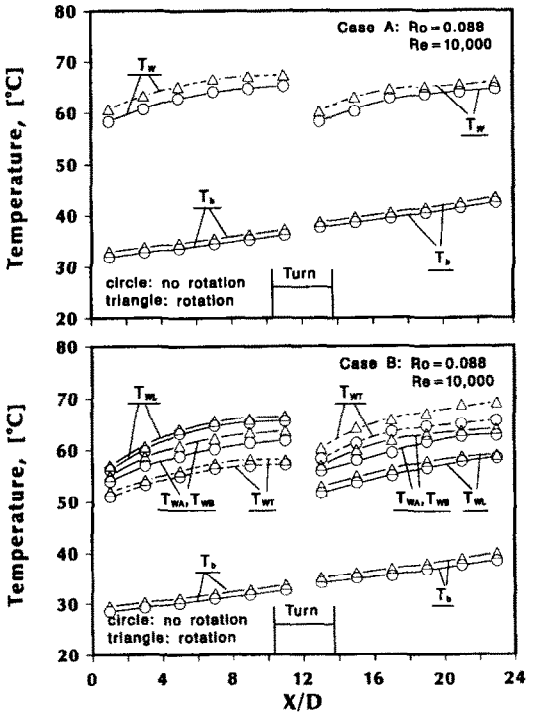

FIG. 3. Variation of the surface and coolant temperature with axial location for Cases A and B.

To reduce the influence of the flow Reynolds number on the heat transfer coefficient with rotation, the local Nusselt number of the present study is normalized by the Nusselt number for a stationary fully developed turbulent flow in a smooth circular tube correlated by Dittus–Boelter/McAdams [18] as:

$$Nu/Nu_0 = (hD/k)/[0.023Re^{0.8}\,Pr^{0.4}] \quad (2)$$

with $Pr = 0.72$. Properties in the Nusselt and the Reynolds numbers are based on the average of the inlet and outlet bulk mean air temperatures. The uncertainty of the local heat transfer coefficient depends on the local wall-to-coolant (air) temperature difference and the net heat input to the air for each copper plate. This uncertainty increases for decreasing both the local wall-to-air temperature difference ($T_w - T_b$) and the net heat input. Based on the method described in ref. [19], the typical uncertainty in the Nusselt number is estimated to be less than 8% for Reynolds numbers larger than 10 000. The maximum uncertainty, however, could be up to 20–25% for the lower heat transfer coefficient at the lowest Reynolds number tested ($Re = 2500$).

EXPERIMENTAL RESULTS AND DISCUSSION

According to refs. [10–13, 16, 17], the Nusselt number in a rotating channel depends on the ratio of the rotating mean radius to channel hydraulic diameter, the ratio of the axial distance to channel hydraulic diameter, Reynolds number, Prandtl number, rotation number, wall-to-coolant density (temperature) difference ratio, flow direction (radial outward flow or radial inward flow), and the rib turbulator geometry (height, spacing, cross section, and orientation, respectively). Their functional relationship can be expressed as:

$$N = f(\bar{R}/D, X/D, Re, Pr, Ro, \Delta\rho/\rho, \text{flow direction, rib geometry}) \quad (3)$$

where $Pr = 0.72$ and $\bar{R}/D = 30$ for the present study. Tests in this study have the following parameter values: $Re = 2500$, 5000, 10 000 and 25 000; $\Omega = 0$, 400 and 800 r.p.m.; combining to produce $Ro = 0.0$, 0.0176, 0.0352, 0.044, 0.088, 0.176 and 0.352. The inlet wall-to-coolant density ratio $(\Delta\rho/\rho)_i$ has the following values: Case A = 0.11; Case B = 0.10, 0.07, and 0.08 for the first pass leading, trailing and side walls, respectively (the reverse is true for the second pass leading and trailing walls); and Case C = 0.10, 0.08, and 0.05 for trailing, leading, and side walls, respectively.

Effect of rotation relative to non-rotation

Figure 4 shows the effect of rotation on the local Nusselt number ratio (Nu/Nu_0) for Case A. Note that the Nusselt number ratio is the ratio of the local Nusselt number with or without rotation to that of fully developed turbulent flow in a smooth circular tube without rotation as shown in equation (2). The results show the local Nusselt number ratios on the trailing and leading ribbed walls are fairly uniform for non-rotation (around 2–4 through the entire two-pass channel for Reynolds numbers between 5000 and 25 000). In the first outflow pass ($0 < X/D < 12$), rotation enhances the Nusselt number ratios on the trailing ribbed wall while it decreases the Nusselt number ratios on the leading ribbed wall, compared to their corresponding non-rotating values. The reverse is true in the second (inflow) pass ($12 < X/D < 24$). This is because rotation creates Coriolis forces that produce secondary cross-stream flows that thin the first pass trailing and the second pass leading wall boundary layers. They also thicken the first pass leading and the second pass trailing wall boundary layers (see the conceptual velocity profile in Fig. 1(b)). Therefore, the heat transfer coefficients for the first pass trailing and the second pass leading walls are higher with rotation than without, whereas the heat transfer coefficients for the first pass leading and the second pass trailing walls are lower with rotation than without. However, as shown in Fig. 4, this rotation effect is reduced as rotation number decreases from $Ro = 0.176$ ($Re = 5000$) to $Ro = 0.0352$ ($Re = 25\,000$).

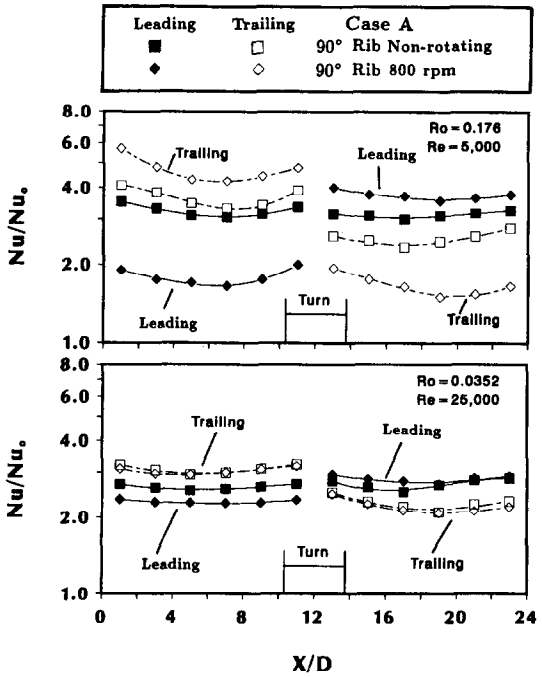

FIG. 4. Effect of rotation on Nusselt number ratio variation for Case A.

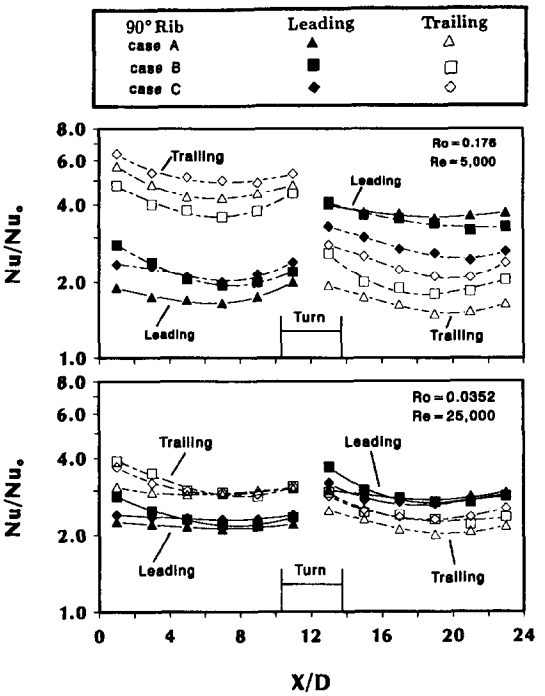

FIG. 5. Effect of wall heating condition on Nusselt number ratio variation for Cases A, B, and C at selected rotation numbers.

Effect of wall heating condition

Figure 5 shows the effect of varying the wall heating condition on the local Nusselt number ratio for rotation numbers $Ro = 0.0352$ ($Re = 25\,000$) and 0.176 ($Re = 5000$). Nusselt number ratios on the lead-

ing ribbed wall for Cases B and C in the first pass ($O < X/D < 12$) are 5–50% higher than those for Case A at $Nu/Nu_0 = 1.8$. The Nusselt number ratios on the trailing ribbed wall for Case B and Case C are 20% lower and 20% higher, respectively, than those for Case A at $Nu/Nu_0 = 4.5$. The Nusselt number ratios on the trailing ribbed wall for Cases B and C in the second pass ($12 < X/D < 24$) are 20–50% higher than those for Case A at $Nu/Nu_0 = 1.7$, while the Nusselt number ratios on the leading ribbed wall for Case B are 20% lower and Case C are 35% lower than Case A at $Nu/Nu_0 = 3.5$. However, as shown in Fig. 5, the wall heating condition effect is reduced with decreased rotation number from $Ro = 0.176$ ($Re = 5000$) to $Ro = 0.0352$ ($Re = 25000$).

The surface heat transfer coefficients on the leading and trailing walls are assumed to be influenced by the relative temperatures of the other channel walls [16,17]. Consider Case C, trailing hotter than leading with unheated side walls. For the first pass (radial outward flow), the wall temperatures (and their related inlet coolant-to-wall density ratios) are $T_{wT} = 60$–$65°C$ (0.10) for trailing, $T_{wL} = 55$–$60°C$ (0.08) for leading, and $T_{wA}, T_{wB} = 45$–$50°C$ (0.05) for the side walls. Due to rotation, the cross-stream secondary vortices carry the cooler fluid from the unheated side walls toward the leading and then the trailing walls (Fig. 1(b)). This creates lower boundary layer temperature on the leading and trailing walls. Therefore, the heat transfer coefficients for Case C are higher than those for Case A of uniform wall temperature condition. For Case B and the first pass with radial outward flow (see Fig. 3 for wall temperatures), the side wall temperature is between the leading and trailing wall temperatures. This still creates lower boundary layer temperature on the leading wall, but when combined with the (hot) leading wall, produces a warmer boundary layer on the trailing wall, relative to Case A. Therefore, the heat transfer coefficients (Nusselt number ratios) for Case B are higher on the leading wall and lower on the trailing wall than those for Case A.

In the second pass (radial inward flow) the direction of the Coriolis force and secondary cross-stream flow is reversed and toward the leading wall (Fig. 1(b)) as compared to toward the trailing wall in the first pass. This causes cooler fluid from the side walls to be carried to the trailing wall for both Cases B and C, relative to Case A. Thus Cases B and C Nusselt number ratios on the trailing wall are increased, relative to Case A. However, for the second pass, the trailing wall heating is large enough to produce a warmer boundary layer on the leading wall for both Cases B and C, relative to Case A. Therefore, Nusselt number ratios on the leading wall are decreased as compared to Case A.

Effect of Reynolds number

Figure 6 shows the effect of Reynolds number on the Nusselt number ratio while holding rotation number at $Ro = 0.088$. The rotation number $Ro = \Omega D/V$ can be held constant by varying rotation speed (Ω) and axial flow velocity (V or Re). The rotation number $Ro = 0.088$ is based on two combinations of Ω and Re: $\Omega = 400$ r.p.m., $Re = 5000$; and $\Omega = 800$ r.p.m., $Re = 10000$. The results show the Nusselt number ratios are unaffected or slightly increase with an increasing Reynolds number at constant rotation number.

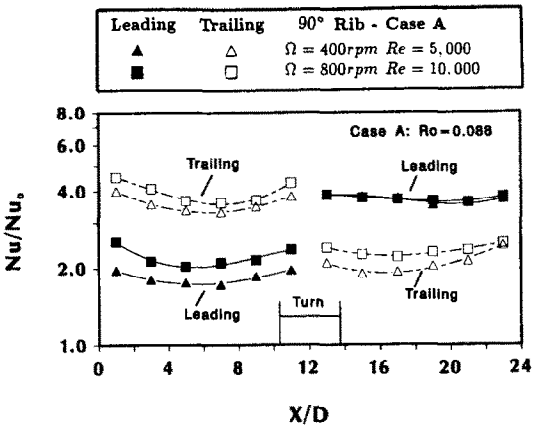

FIG. 6. Effect of Reynolds number on Nusselt number ratio variation for Case A.

Effect of rotation number and wall heating condition

Figure 7 shows the effect of rotation number on the Nusselt number ratio at six selected channel axial locations for the three studied wall heating conditions. For comparison to smooth wall results, the data of ref. [17] for Case A, uniform wall temperature, are also included. The results show that, for the smooth wall channel, the first pass trailing wall Nusselt number ratio increases with an increasing rotation number, whereas, the first pass leading wall Nusselt number ratio decreases and then increases with an increasing rotation number. The reverse is true for the second pass, radial inward flow. Results also show the trend of the differences between the leading and trailing Nusselt number ratios decreasing in the second pass as compared to the first pass. This is because the inertia force pushing the air through the channel is aided by the radial buoyancy force in the first pass and then is partially counteracted by it in the second pass. Therefore, the second pass streamwise driving force (inertia-radial buoyancy), and thus Coriolis force, is reduced, and thus the differences between leading and trailing Nusselt number ratios are smaller.

Figure 7 shows that, for the ribbed wall channel, the first pass leading and second pass trailing wall Nusselt number ratios for Cases B and C are up to 50% higher than those for Case A. While the first pass trailing wall Nusselt number ratios for Case C are up to 20% higher, the Case B is up to 20% lower than those for Case A. The second pass leading wall Nusselt number ratios for Cases B and C are within 35% of those for Case A. The second pass trailing wall Nusselt number ratios for Cases B and C are up to 50% higher

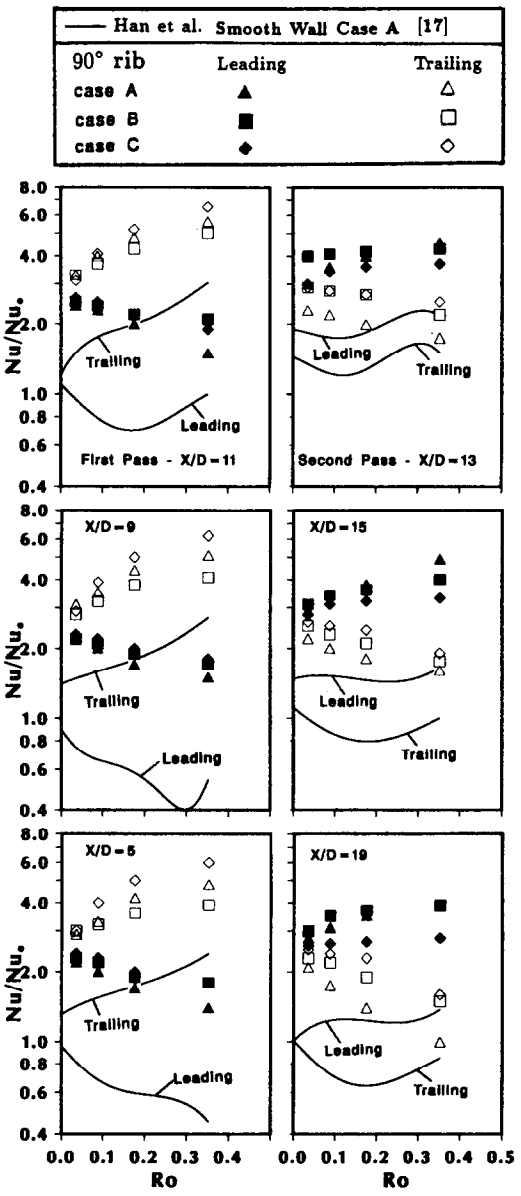

FIG. 7. Effect of rotation number on Nusselt number ratio variation at selected axial locations for Cases A, B, and C.

than those for Case A. Furthermore, ribs greatly enhance the wall Nusselt number ratios for the entire two pass channel while under rotation, compared to their corresponding smooth wall results. The factor increase is roughly 2 or 3.

Not only do wall heating condition and rotation number affect local surface heat transfer coefficients but so does rib orientation. For the 90° transverse ribs, Nusselt number ratio variation among the three wall heating conditions increases with increasing rotation number and is up to 50% as shown in Fig. 7. For the 60° angled ribs [20], this variation (not shown here) also increases with rotation number but is up to 100%. For the smooth wall channel [16,17], this variation does not uniformly increase with rotation number and is up to 100%. This implies that the uneven wall temperatures of the wall heating conditions, Cases B and C, have less effect on heat transfer (Nusselt number ratio) for 90° transverse ribs than for the 60° angled ribs and for the smooth wall channel. This may be because the 90° transverse ribs reduce the effect of rotation-induced secondary flows, as compared to that of the 60° angled ribs and the smooth wall channel.

Effect of rotation number and rib geometry comparison

Figure 8 shows the effect of rotation number on the Nusselt number ratio at six selected channel axial locations (the first pass $X/D = 5, 9, 11$, and the second pass $X/D = 13, 15, 19$ or $X'/D = 1, 3, 7$) for Case A, uniform wall temperature. Experimental results for

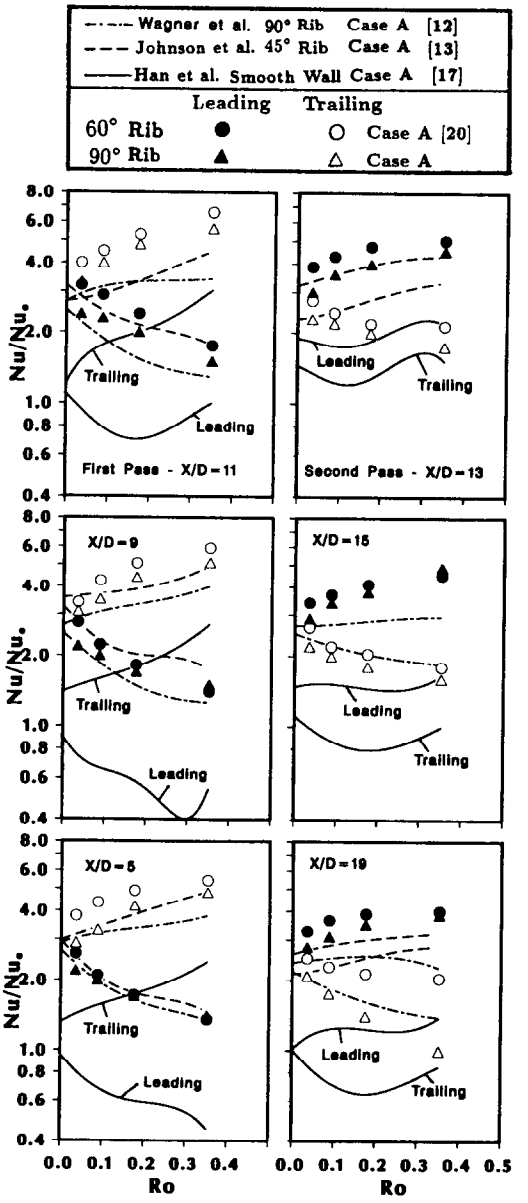

FIG. 8. Effect of rotation number on Nusselt number ratio variation at selected axial locations for Case A, and comparison with the previous results.

Case A from four previous investigations [12, 13, 17, 20] are included for comparison. The results for 90° ribs [12] and 45° ribs [13] are based on the following conditions and locations: Ro calculated from $Re = 25\,000$ and varying rotation speeds, $(\Delta\rho/\rho)_i = 0.13$, $\bar{R}/D = 49$, the first pass (radial outward flow) $X/D = 4.6$, 8.5, 12.4 (no ribs for $X/D < 3$), and the second pass (radial inward flow) $X'/D = 2.0$ (45° rib) or 3.0 (90° rib), 6.0 (45° rib) or 7.0 (90° rib), where X' starts at the second pass inlet. The ribs are semicircular in cross section, have a rib height ratio of $e/D = 0.10$, and have a rib spacing ratio of $P/e = 10$.

Figure 8 shows the comparison between the present 90° rib data and ref. [12] 90° rib results for the case of uniform wall temperature condition. In the first pass, the present Nusselt number ratios on the leading wall agree with those of ref. [12], while the present Nusselt number ratios on the trailing wall are significantly higher than those of ref. [12] over the range of rotation numbers studied. In the second pass, the present data on the leading surface are higher; however, the present data on the trailing surface are slightly lower than those of ref. [12]. The same observation is true for the comparison between the 60° ribs [20] and the 45° ribs [13] (ignoring the small angle difference). The difference between these two sets of studies may be explained as follows. The ribs for refs. [12, 13] are semicircular in cross section and have a rib height ratio of $e/D = 0.10$. The ribs for ref. [20] and this study are square in cross section and have a rib height ratio of $e/D = 0.125$. Since rotation creates a thinner boundary layer on the first pass trailing wall and a thicker boundary layer on the first pass leading wall, it is expected that the rib height, rib shape, and rib orientation (angle) have a more significant effect on the thinner trailing wall boundary layer than that on the thicker leading wall boundary layer. Sharper and taller ribs are more effective in tripping thin boundary layers. Therefore, the Nusselt number ratios on the first pass trailing wall for the 60° ribs [20] and the present 90° ribs are higher than those of the 45° ribs [13] and the 90° ribs [12], respectively. Thus the Nusselt number ratios on the first pass leading ribbed wall (thicker boundary layer) are about the same. Similarly, Nusselt number ratios on the leading wall (thinner boundary layer) for the square ribs are higher in the second pass, but the Nusselt number ratios on the trailing wall (thicker boundary layer) for all studies are about the same. However, the 60° rib [20] and the present 90° rib data on the second pass trailing wall are relatively lower than those of the 45° rib [13] and the 90° rib [12], respectively, particularly at the largest axial location $X/D = 19$. This may be due to the different combined effects of rotation, rib orientation, and second pass entrance geometry (ref. [20] and present study-sharp 180° turn with ribs versus refs. [12, 13] gradual 180° bend without ribs).

In addition, Fig. 8 shows the effect of rib angle. The 60° rib data [20] are higher than the present 90° rib data, and similarly, the 45° rib data [13] are higher than their corresponding 90° rib data [12]. This may be explained as follows. The combination of the inertia driving (streamwise) and the Coriolis (cross-stream) forces produce a spiral fluid flow path and thus spirally developing boundary layers along the channel (Fig. 1(b)). The skewed ribs are believed to be oriented about the local flow in a direction more effective to trip the boundary layers, than are the 90° transverse ribs. Therefore, skewed ribs produce higher Nusselt number ratios than 90° ribs, especially on the first pass trailing and second pass leading walls (thinner boundary layers) of the channel.

Effect of buoyancy parameter and wall heating condition and comparison

A buoyancy parameter $(\Delta\rho/\rho)(R/D)(Ro)^2$ is used to consider combined effects of Coriolis and buoyancy forces on heat transfer [10–13, 16, 17, 20]. The buoyancy parameter includes the effects of the local coolant-to-wall density ratio ($(\Delta\rho/\rho) = (T_w - T_b)/T_w$, related to buoyancy force), secondary cross-stream flow (due to Coriolis force, related to Ro), and rotating radius-to-hydraulic diameter ratio (R/D, related to buoyancy force). Figure 9 shows the Nusselt number ratio variation with buoyancy parameter at selected axial locations for the present 90° rib data for wall heating conditions A, B and C. The results for smooth wall channel [17], and for 90° ribs [12] and 60° ribs [20] are also included for comparison. The buoyancy parameter effect on the Nusselt number ratios show similar trends as those presented and discussed in Figs. 7 and 8. The wall heating condition has an effect on all of the walls because the rotation induced secondary flows carry cooler or warmer fluid from other walls, as discussed above.

CONCLUDING REMARKS

The influence of wall heating condition on the local surface heat transfer coefficients in a rotating two-pass square channel with 90° transverse ribs on the leading and the trailing walls has been observed for rotating numbers from 0.0352 to 0.352 and Reynolds numbers from 2500 to 25 000. The findings are as follows.

1. The trailing wall Nusselt number ratios for the first pass (Case A) are higher than the leading wall Nusselt number ratios, and increase with increasing rotation numbers. The leading wall Nusselt number ratios decrease with an increasing rotation number. The rotating ribbed wall heat transfer coefficients are 2 to 3 times higher than their corresponding rotating smooth wall values. The difference between the leading and trailing wall Nusselt number ratios increases with increasing rotation number. This is because the rotation creates a thinner boundary layer on the trailing wall and a thicker boundary layer on the leading wall.

2. The leading wall Nusselt number ratios in the second pass (Case A) are higher than the trailing wall

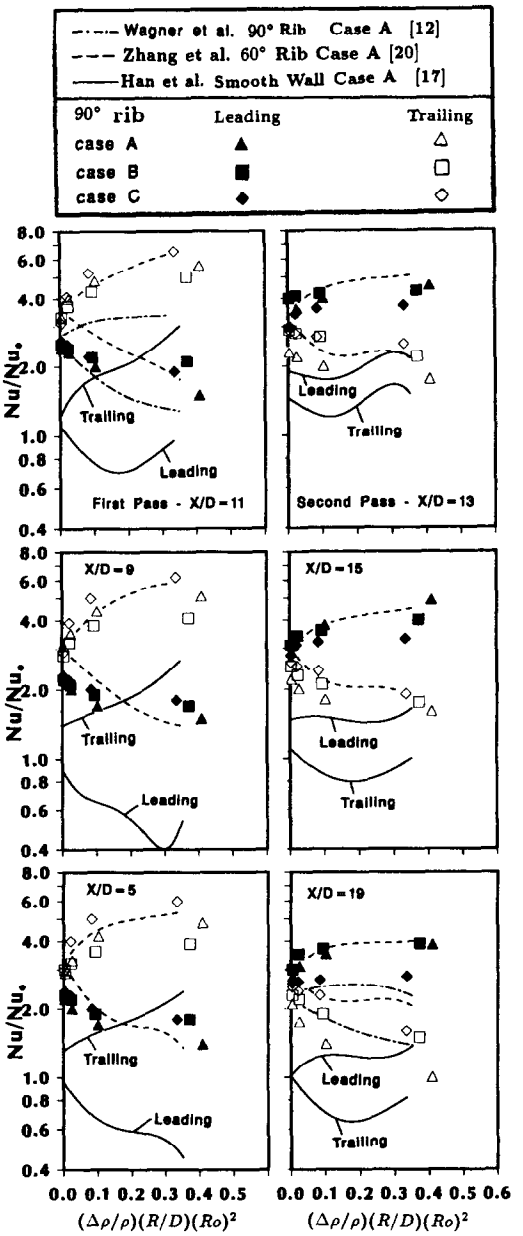

FIG. 9. Effect of buoyancy parameter on Nusselt number ratio at selected axial locations for Cases A, B, and C, and comparison with previous results.

Nusselt number ratios due to a reversal of the Coriolis force direction. The leading wall Nusselt number ratios increase and the trailing wall Nusselt number ratios decrease with increasing rotation number. Again, the rotating ribbed wall heat transfer coefficients are higher than their corresponding rotating smooth wall values. The difference between the leading and trailing wall Nusselt number ratios in the second pass is smaller than that in the first pass because the rotation-induced buoyancy force aids the inertia force in the first pass and opposes the inertia force in the second pass.

3. In the first pass, the Nusselt number ratios on the leading wall with 90° ribs for Cases B and C are up to 50% higher than those for Case A. In the second pass, the Nusselt number ratios on the trailing wall with 90° ribs for Cases B and C are also up to 50% higher than those for Case A. This is because the rotation-induced secondary flows carry cooler fluid from the side walls toward the leading wall (in the first pass), also from the side walls towards the trailing wall (in the second pass). These wall heating effects for the 90° ribs are less than those for the 60° angled ribs [20] and for the smooth wall channel [17], respectively.

4. The trends of the Nusselt number ratio versus the rotation number for the present 90° ribs agree with the previous 90° ribs [12] for Case A. However, the Nusselt number ratios on the first pass trailing and second pass leading walls of this study are higher than those of ref. [12]. This is because the relatively thinner boundary layers on these walls are affected more by the taller and square cross section ribs of this study. Conversely, the relatively thicker boundary layers on the first pass leading and second pass trailing walls are only slightly affected by the difference in rib geometry.

Acknowledgement—This investigation was supported by the Texas Higher Education Coordinating Board (Energy Research in Application Programs—1990, 999903-050, TEES 70730).

REFERENCES

1. J. C. Han, Heat transfer and friction in channels with two opposite rib-roughened walls, *ASME J. Heat Transfer* **106**, 774–781 (1984).
2. J. C. Han, Heat transfer and friction characteristics in rectangular channels with rib turbulators, *ASME J. Heat Transfer* **110**, 321–328 (1988).
3. Y. Mori, T. Fukada and W. Nakayama, Convective heat transfer in a rotating radial circular pipe (2nd report), *Int. J. Heat Mass Transfer* **14**, 1807–1824 (1971).
4. R. J. Clifford, W. D. Morris and S. P. Harasgama, An experimental study of local and mean heat transfer in a triangular-sectioned duct rotating the orthogonal mode, *ASME J. Engng Gas Turbines Power* **106**, 661–667 (1984).
5. S. P. Harasgama, and W. D. Morris, The influence of rotation on the heat transfer characteristics of circular, triangular, and square-sectioned coolant passages of gas turbine rotor blades, *ASME J. Turbomach.* **110**, 44–50 (1988).
6. J. Guidez, Study of the convective heat transfer in rotating coolant channels, *ASME J. Turbomach.* **111**, 43–50 (1989).
7. C. Y. Soong, S. T. Lin and G. J. Hwang, An experimental study of convective heat transfer in radially rotating rectangular ducts, *ASME J. Heat Transfer* **113**, 604–611, (1991).
8. M. E. Taslim, A. Rahman and S. D. Spring, An experimental investigation of heat transfer coefficients in a spanwise rotating channel with two opposite rib-roughened walls, *ASME J. Turbomach.* **113**, 74–82 (1991).
9. M. E. Taslim, L. A. Bondi and D. M. Kercher, An experimental investigation of heat transfer in an orthogonally rotating channel roughened with 45 degree crisscross ribs on two opposite walls, *ASME J. Turbomach.* **113**, 346–353 (1991).
10. J. H. Wagner, B. V. Johnson and T. J. Hajek, Heat transfer in rotating passages with smooth walls and rad-

ial outward flow, *ASME J. Turbomach.* **113,** 42–51 (1991).
11. J. H. Wagner, B. V. Johnson and F. C. Kopper, Heat transfer in rotating serpentine passages with smooth walls, *ASME J. Turbomach.* **113,** 321–330 (1991).
12. J. H. Wagner, B. V. Johnson, R. A. Graziani and F. C. Yeh, Heat transfer in rotating serpentine passages with trips normal to the flow, *ASME J. Turbomach.* **114,** 847–857 (1992).
13. B. V. Johnson, J. H. Wagner, G. D. Steuber and F. C. Yeh, Heat transfer in rotating serpentine passages with trips skewed to the flow, *ASME J. Turbomach.* **116,** 113–123 (1994).
14. W. J. Yang, N. Zhang and J. Chiou, Local heat transfer in a rotating serpentine flow passage, *ASME J. Heat Transfer* **114,** 354–361 (1992).
15. C. Prakash and R. Zerkle, Prediction of turbulent flow and heat transfer in a radially rotating square duct, *ASME J. Turbomach.* **114,** 835–846 (1992).
16. J. C. Han and Y. M. Zhang, Effect of uneven wall temperature on local heat transfer in a rotating square channel with smooth walls and radial outward flow, *ASME J. Heat Transfer* **114,** 850–858 (1992).
17. J. C. Han, Y. M. Zhang and K. Kalkuehler, Uneven wall temperature effect on local heat transfer in a rotating two-pass square channel with smooth walls, *ASME J. Heat Transfer* **115,** 912–920 (1993).
18. W. M. Rohsenow and H. Choi, *Heat, Mass and Momentum Transfer*, pp. 192–193. Prentice-Hall, Englewood Cliffs, New Jersey, U.S.A. (1961).
19. S. J. Kline and F. A. McClintock, Describing uncertainties in single-sample experiments, *Mech. Engng* **75,** 3–8 (1953).
20. Y. M. Zhang, J. C. Han, J. A. Parsons and C. P. Lee, Surface heating effect on local heat transfer in a rotating two-pass square channel with 60° angled rib turbulators, ASME Paper No. 93-GT-336 (1993).